Spectroscopic study of electrons emitted in Ar^{q+} $(8 \leq q \leq 16)$ on Ar at $2.3q$ keV collision energy

J. Vancura, P. J. Mucha, and V. O. Kostroun
Nuclear Science and Engineering Program, Ward Laboratory, Cornell University, Ithaca, New York 14853
(Received 27 September 1995)

The spectra of electrons emitted in Ar^{q+} on Ar $(8 \leq q \leq 16)$ collisions at $2.3q$ keV were measured in the 30–400-eV energy range. Ar^{q+} ions were produced by the Cornell superconducting solenoid, cryogenic electron-beam ion source, and the emitted electrons analyzed by a $\sqrt{\pi}/2$ cylindrical electrostatic analyzer at 90° to the ion beam. The observed spectral features are interpreted in terms of energy differences between total electronic energies of final states of the collision system $[Ar^{q+}+$ (electron configuration)$] + Ar^{r+}$ and the $Ar^{q+}+$ Ar ground-state total electronic energy. The measured spectra appear to have a common interpretation.

PACS number(s): 34.50.Fa, 34.90.+q, 34.70.+e, 82.30.Fi

I. INTRODUCTION

Spectroscopic investigations of electron emissions in low-energy, highly charged ion-atom collisions under single-collision conditions were reported by Bordenave-Montesquieu *et al.* [1], who investigated electrons emitted in the decay of autoionizing states $N^{5+}(nln'1')$ $(n=2,3,4$ and $n' \geq n)$ formed in collisions of N^{7+} with He and H_2 at 4.9 keV/amu. The number of systems that has been investigated since is quite large, with emphasis placed on bare and H- and He-like ions of C, N, and Ne incident on H_2 and He [2–8]. Double-electron capture in $10q$ keV $Ar^{8+,9+}$ collisions with He atoms was investigated by electron spectroscopy by Hutton *et al.* [9].

Multiple-electron capture in low-energy, highly charged Ar-ion collisions with Ne and Ar was investigated with electron spectroscopy by Posthumus and Morgenstern [10,11]. Unlike double-electron capture from H_2 and He, which results in electron emission from only a few autoionizing states of the projectile formed in capture, multiple-electron capture from many-electron targets gives rise to electron spectra that are much more difficult to interpret because of the large number of excited projectile capture states possible. Furthermore, in a purely spectroscopic measurement, one cannot distinguish in an unambiguous manner between autoionization from states populated directly in capture and nonradiative decays from states populated in the deexcitation of higher-energy, multiply excited states.

In collisions of low-energy, highly charged ions with many-electron targets, most of the projectiles undergo collisions in which the charge state q, observed long after the collision, decreases by one unit only. For example, for Ar^{q+} on Ar, collisions involving projectile charge-state changes by two units are less frequent, and by more than two units are quite rare [12]. At the same time, the recoil target ion charge state distribution contains ions whose charge can range from one to eight [13]. Since singly charged recoil ions account only for about one half of the ions observed [12], a significant fraction of the collisions has to be accompanied by electron emissions. By looking at the number and energy distribution of the electrons emitted, one might expect to learn something about collisions between low-energy, highly charged ions and many-electron target atoms.

Unfortunately, the large number of target electrons which can be captured by the projectile complicates the interpretation of the observed electron spectra. There are at least two ways of approaching this problem of interpretation. One approach, taken by Posthumus and Morgenstern [10], is to measure energy-analyzed electrons in coincidence with target recoil ions. In this manner, it is possible to obtain partial electron energy spectra, each spectrum corresponding to a specific charge state of the target ion, and hence to the number of electrons initially captured (assuming that in capture the target is not ionized or excited to a state that decays nonradiatively). In this paper we report on a somewhat different method of attack on the problem of interpretation. The method is based on a systematic study of the electron spectra emitted in Ar^{q+} on Ar $(8 \leq q \leq 16)$ collisions at $2.3q$ keV. As far as we have been able to determine, this is the first investigation of electron emissions in low-energy, ion-atom collisions involving projectile charges q greater than ten.

II. EXPERIMENT

In the present experiment, Ar^{q+} $(8 \leq q \leq 16)$ ions were produced by the Cornell superconducting solenoid, cryogenic electron-beam ion source (CEBIS) [14], and extracted at 2.3 kV. The pertinent experimental arrangement is shown in Fig. 1. Magnetically selected Ar charge states passed through a 10-cm-long gas cell which contained argon at 1.0×10^{-3}-mbar pressure. The gas cell was similar in design to that used in an earlier experiment to measure absolute total, and one- and two-electron transfer cross sections in Ar^{q+} on H_2 and He collisions [15]. The ion beam transmitted through the gas cell could be charge state analyzed by a $\pi/\sqrt{2}$ electrostatic analyzer. Inside the gas cell, the ion beam was surrounded by a cylinder made from stainless-steel mesh of 80% transparency. The mesh was insulated from ground, and its potential with respect to the grounded gas cell could be varied to accelerate or decelerate the electrons emitted in Ar^{q+} on Ar collisions.

Electrons emitted from a 1.5-cm-long portion of the gas-ion beam were analyzed at 90° to the incident-beam direction by a $\pi/\sqrt{2}$ cylindrical electrostatic analyzer with its en-

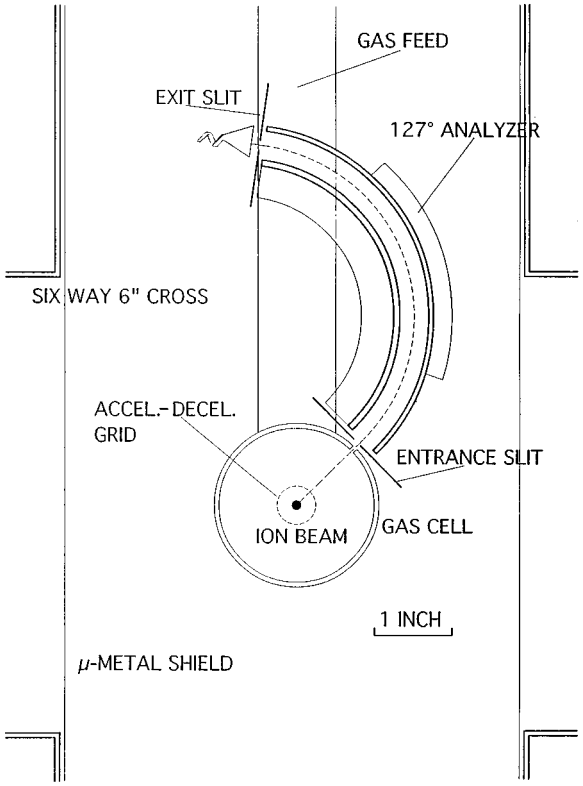

FIG. 1. Experimental arrangement used to measure electron spectra emitted in $Ar^{q+}(8 \leq q \leq 16)$ on Ar collisions at $2.3q$ keV.

trance slit parallel to the beam. The analyzer was made from aluminum which was copper and then gold plated. The outer and inner radii of the analyzer are 6.03 and 5.02 cm, respectively. The electrons were detected by a 1-cm-diameter cone channeltron detector. The gas cell and cylindrical electrostatic analyzer were mounted on a 20-cm-diameter stainless-steel vacuum flange attached to a 15-cm six-way cross vacuum chamber. The system was pumped on by a Varian Cryostack 8 cryopump, and the background pressure, with no gas in the cell, was 1.0×10^{-8} mbar. The analyzer was shielded by a thin μ-metal cylinder, 12 cm in diameter and 40 cm long.

The electron spectrometer was located near the focus of the 90° bending magnet used to charge select the ion beam extracted from CEBIS. At this position, the measured ion-beam diameter was 1.5 mm. The beam diameter, together with a 1.0-mm-wide analyzer entrance slit, the analyzer and gas cell dimensions, and the 10-mm-diameter channeltron detector placed directly behind the exit slit, set the energy resolution $\Delta E/E$ at 0.025.

The operation of the $\pi/\sqrt{2}$ cylindrical electrostatic analyzer was verified by recording argon $L_{2,3}MM$ Auger-electron spectra excited by 3-keV electron impact, Fig. 2. The 3-keV electron beam was generated by an electron gun from a Westinghouse Electric Corp. 40.6-cm WX-30810P cathode ray tube, mounted at the entrance to the apparatus where the ion beam normally entered. The electron beam transmitted through the chamber was observed on a fluorescent screen. From the measured screen beam size (diameter less than 1 mm), and the physical dimensions of the apparatus, the width of the unresolved $L_2M_{2,3}M_{2,3}$ peaks is consistent with the calculated resolution of the system, 5 eV at 205 eV. [The most intense peaks in the spectrum are the $L_2M_{2,3}M_{2,3}$ (^1D) peak at 203.31 eV and the (^3P) peak at 205.05 eV [16,17].]

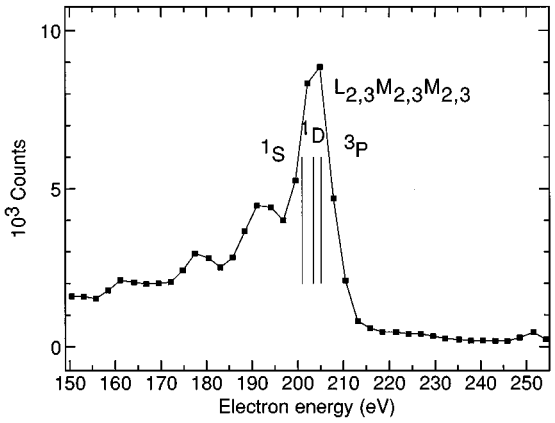

FIG. 2. Auger $L_{2,3}M_{2,3}M_{2,3}$ electron spectrum excited by 3-keV electron impact and recorded using the apparatus shown in Fig. 1.

To record the electron spectra emitted in Ar^{q+} on Ar collisions, the potentials $\pm V/2$ on the inner and outer electrodes of the electron analyzer were set to transmit 45-eV electrons, and the emitted electrons were either accelerated or decelerated to this energy by varying the potential applied between the cylindrical mesh surrounding the ion beam and the grounded gas cell. The fixed potential difference between the plates of the electrostatic analyzer ensured constant transmission through the analyzer.

The geometry used to analyze the emitted electrons was chosen to maximize the detection solid angle subtended by a line source parallel to the entrance slit of a cylindrical electrostatic analyzer. In this case, the angular divergence in the analyzing plane is determined by the length of the line source, the source to detector distance, and the detector diameter. The disadvantage of this geometry is that at 90° observation angle, the Doppler shift variation of electron energy with angle is the greatest. However, at a projectile velocity of less than 0.2 a.u., corresponding to a 36.8-keV Ar^{16+} ion beam, the Doppler broadening of 100–400-eV electrons due to a $\pm 3.5°$ acceptance angle around 90° is less than 0.4 eV.

III. RESULTS

Electrons emitted in Ar^{q+}-Ar collisions in the 30–400-eV energy range were recorded for projectile charge states from 8 to 16 inclusive. The results are shown in Figs. 3(a)–3(i). In the figure, the electron spectra were normalized to the same projectile beam intensity in order to show how the electron intensity increases with projectile charge state. A small but constant background due to electrons produced in other parts of the apparatus and scattered into the detector was subtracted from each of the spectra. For each incident projectile charge state, the ion beam transmitted through the cell was charge state analyzed to ensure that the transmitted beam contained mostly one and two electron transfer peaks. Each spectrum shown is a series of several runs recorded over a period of 1–6 h.

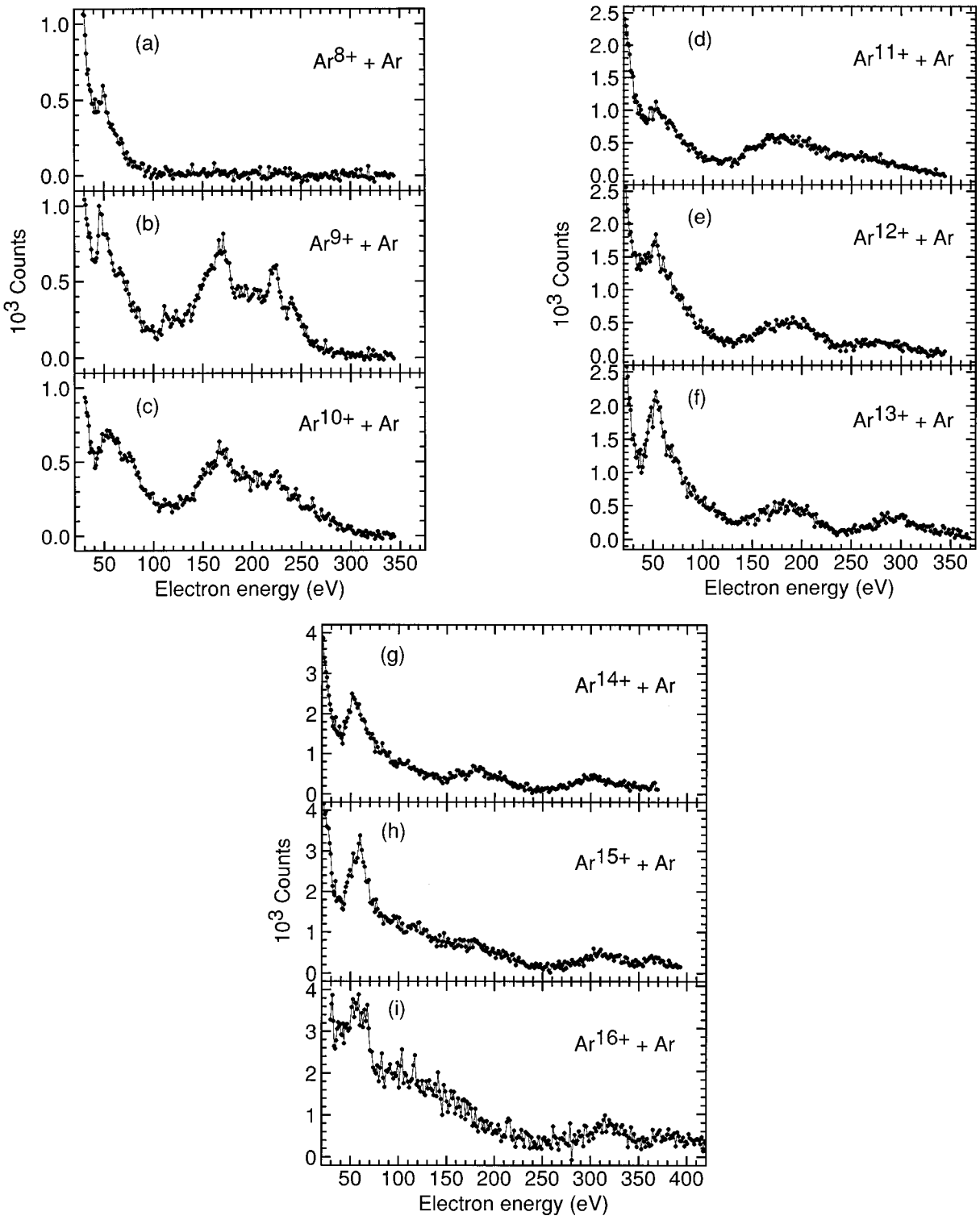

FIG. 3. (a)–(i) spectra of electrons emitted in $Ar^{q+}(8 \leqslant q \leqslant 16)$ on Ar collisions at 2.3q keV. The spectra were normalized to the same number of incident ions, and a small constant background was subtracted from each. Note the marked similarities between (b) and (c), and among (d)–(f) and (g)–(i).

Figure 4 compares our electron spectrum for Ar^{9+} on Ar at 2.3q keV collision energy with that obtained by Posthumus and Morgenstern at 12.0q keV [10]. Clearly the spectra are quite similar. Our spectrum is a little bit more smeared out than that of Posthumus and Morgenstern. We do not know whether or not this is an instrumental effect, their resolution being better than ours, or an effect due to the lower collision velocity in our experiment. (To bring the main features into alignment on the same energy scale, the spectra had to be shifted by 8 eV relative to one another.)

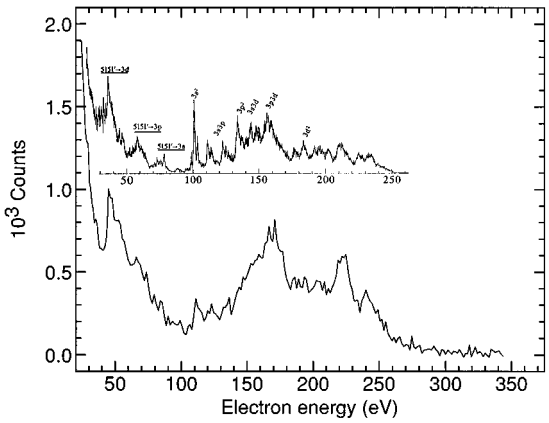

FIG. 4. Comparison between our measured electron spectrum emitted in $2.3q$ keV Ar^{9+} on Ar collisions and that of Posthumus and Morgenstern [10] emitted at $12.0q$ keV (inset). To bring the major peaks into alignment, the spectra had to be shifted by 8 eV relative to one another.

IV. DISCUSSION

The total electronic ground-state energies of the Ar^{q+} on Ar collision system before and after the collision determine the net change in the internal energy of this system. This change in internal energy appears as (i) a change in the total kinetic energy of the nuclei, and (ii) as the energy of photons and the kinetic energy of electrons emitted during and after the collisions. If r electrons are captured from the target by the projectile in the collision,

$$Ar^{q+} + Ar \rightarrow (Ar^{(q-r)+})^* + (Ar^{r+}). \tag{1}$$

In turn, the excited projectile and target deexcite, so that

$$(Ar^{(q-r)+})^* \rightarrow Ar^{(q-s)+} + (r-s)e^- + (\text{photons}) \tag{2a}$$

and

$$(Ar^{r+})^* \rightarrow Ar^{(r+t)+} + te^- + (\text{photons}). \tag{2b}$$

In what follows, we neglect target excitation that deexcites by nonradiative transitions, and set $t=0$ in (2b).

Let $E(Ar^{q+})+E(Ar)$ be the total electronic energy of the ground state of the system at infinite separation before the collision, and $E(Ar^{(q-s)+})+E(Ar^{r+})$ the total electronic ground-state energy of the system at infinite separation after the collision. Ultimately, the energy difference

$$[E(Ar^{q+})+E(Ar)]-[E(Ar^{(q-s)+})+E(Ar^{r+})] \tag{3}$$

has to be shared by the nuclei and the electrons and photons emitted during, or long after, the collision.

From Eq. (3) we can calculate the maximum recoil charge that will be observed in the collision. For example, for one electron transfer, unaccompanied by target excitation, i.e., for the capture of r electrons in the collision, of which only one is permanently retained by the projectile, we require that

$$E(Ar^{r+}) \leqslant [E(Ar^{q+})+E(Ar)-E(Ar^{(q-1)+})]. \tag{4}$$

With the help of the general Hartree-Fock program HF86 [18], we obtain the following values for the total relativistic electronic energies: $E(Ar^{8+})=-507.68$ a.u., $E(Ar^{7+})=-512.94$ a.u., and $E(Ar)=-528.57$ a.u. From Eq. (4) we obtain that $E(Ar^{r+}) \leqslant -523.32$ a.u. Since $E(Ar^{4+})=-523.42$, the maximum recoil charge state that is energetically allowed with Ar^{7+} is $4+$. If we consider two-electron transfer, $E(Ar^{(q-1)+})$ in Eq. (4) has to be replaced by $E(Ar^{(q-2)+})$, and since $E(Ar^{(q-1)+}) < E(Ar^{(q-2)+})$, the maximum recoil charge r observed in this case will be greater. For $E(Ar^{6+})=-517.43$ a.u., $E(Ar^{r+}) \leqslant -518.81$ a.u., and since $E(Ar^{5+})=-520.74$, the maximum recoil charge state energetically allowed with Ar^{6+} is $5+$. This is consistent with the measured recoil ion charge-state distribution for Ar^{8+} on Ar collisions [13], Ar^{1+}, 0.428 ± 0.002; Ar^{2+}, 0.209 ± 0.002; Ar^{3+}, 0.175 ± 0.001; and Ar^{4+}, 0.089 ± 0.001. Furthermore, since the fraction of Ar^{7+}, Ar^{6+}, and Ar^{5+} final charge projectiles observed is 0.865 ± 0.032, 0.128 ± 0.028, and 0.006 ± 0.005, respectively [12], the maximum recoil charge state observed is accounted for.

From the total electronic energies of excited atoms or ions, we can calculate Q values for the capture of r electrons during the collision. (The Q value is the change in the total kinetic energy of the nuclear translational motion of the collision system that accompanies capture.) The Q value for single-electron capture into a state nl of the projectile is

$$Q\{(nl)\} = \{E(Ar^{q+})+E(Ar)\} - \{E[Ar^{q+}+(nl)] + E(Ar^{1+})\}, \tag{5a}$$

that for the capture of two electrons into the state $(nl)(n'l')$ is

$$Q\{(nl)(n'l')\} = \{E(Ar^{q+})+E(Ar)\} - \{E[Ar^{q+}+(nl)(n'l')]+E(Ar^{2+})\}, \tag{5b}$$

and so on.

If one assumes that the electrons transferred from the target to the projectile during the collision form an excited state that deexcites some time after the collision partners have separated, then we can use the energies of separated atoms and ions to fill in the energy levels between the ground states of the collision system long before and after the collision. For nonradiative transition rates Γ of the order of 10^{-3} a.u. or less, 0.15-a.u. collision velocity, and 20-a.u. internuclear separation, $\Gamma_t=0.133$, and $\exp(-\Gamma_t)=0.88$. In this case very few decays take place while the collision partners are interacting strongly, and the above assumption for calculating Auger energies is reasonable.

In what follows, it is convenient to measure the total electronic energies at infinite separation of singly, doubly, etc. excited states of ions accompanied by recoils of charge r, with respect to the initial ground-state total electronic energy of the $Ar^{q+}+Ar$ system. That is, let

$$E[q,r,(nl)] \equiv \{E[Ar^{q+}+(nl)]+E(Ar^{r+})\} - \{E(Ar^{q+})+E(Ar)\}, \tag{6a}$$

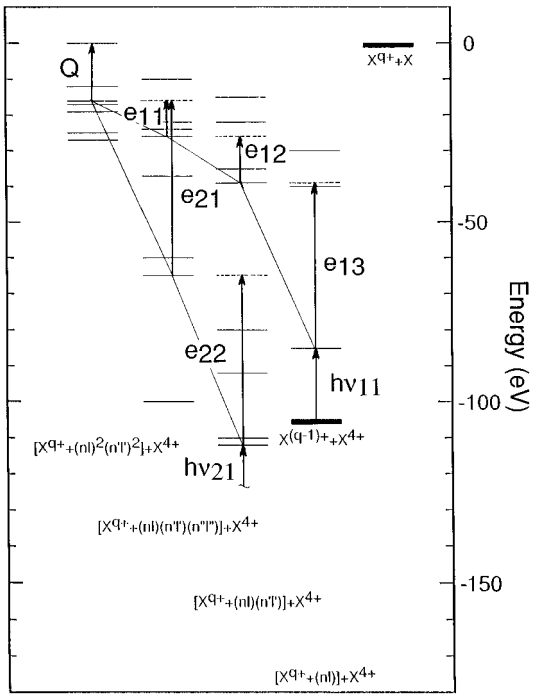

FIG. 5. Schematic energy-level diagram of a hypothetical $X^{q+}+X$ collision system at infinite separation. The energies plotted, $E[q,r,\text{config.})]=\{E[X^{q+}+(\text{config.})]+E(X^{r+}\}-\{E(X^{q+})+E(X)\}$, are the total electronic energies of the collision system referenced to the $X^{q+}+X$ ground-state energy. The collision Q value for the capture of four electrons and two possible decay paths together with electron and photon energies are shown. Path 1 leads to the $X^{(q-1)+}+X^{4+}$, and path 2 to the $X^{(q-2)+}+X^{4+}$ ground state.

$$E[q,r,(nl)(n'l')]\equiv\{E[\mathrm{Ar}^{q+}+(nl)(n'l')]+E(\mathrm{Ar}^{r+})\}-\{E(\mathrm{Ar}^{q+})+E(\mathrm{Ar})\}, \tag{6b}$$

etc. Note that the energies $E[q,1(nl)(n'l')]$, $E[q,2,(nl)(n'l')]$, ... associated with recoil ions of charge 1+, 2+, ... are all different, even though the Ar^{q+} projectile captured electron configuration $(nl)(n'l')$ is the same in all cases.

In this notation, the energy of an Auger electron emitted in the deexcitation of the state of energy $E[q,r,(nl)(n'l')(n''l'')]$ to that of energy $E[q,r,(nl)(n'l')]$ is $E[q,r,(nl)(n'l')(n''l'')]-E[q,r,(nl)(n'l')]$. The energy of a photon emitted in the transition from the state of energy $E[q,r,(n'l')]$ to that of energy $E[q,r,(nl)]$ is $E[q,r,(n'l')]-E[q,r,(nl)]$. Figure 5 illustrates this energy-level scheme and possible transitions for a hypothetical $X^{q+}+X$ system which decays to the ground state of the $X^{(q-1)+}+X^{4+}$ system. The decay scheme is what we believe to be typical of that observed for the capture of a larger number of electrons of which only one is retained by the projectile. For a given Q associated with the capture of four electrons, path 1 involves the emission of two low-energy electrons e_{11} and e_{12}, plus an energetic electron e_{13}. The final transition to the ground state of $X^{(q-1)+}+X^{4+}$ emits a photon of energy $h\nu_{11}$. Path 2 involves the emission of two energetic Auger electrons e_{21} and e_{22}, to a doubly excited state of the $X^{(q-2)+}+X^{4+}$ system which lies just below the ground state of the $X^{(q-1)+}+X^{4+}$ system. This excited state and all other $[X^{q+}+(nl)(n'l')]+X^{4+}$ states lying below it have to deexcite by photon emission, of which only the first, $h\nu_{21}$, is shown. Path 2 leads to the $X^{(q-2)+}+X^{4+}$ ground state.

In an attempt to understand the observed electron energy spectra in Figs. 3(a)–3(i), we have calculated the energies of a number of excited states $E[q,r,(\text{electron configuration})]$ for the collision systems Ar^{q+} $(8\leqslant q\leqslant 16)+\mathrm{Ar}$ and $r=1-4$. The energies were calculated using the general Hartree-Fock code HF86 [18]. In order to keep the calculations tractable we considered only s and p states, since for the highly excited states of interest, the higher angular momentum states lie closer in energy to the p state than the s-p separation. In the same vein, we have only considered configurations, and not the possible terms.

The very large number of energy states calculated presents a problem as to how best display the results. We chose the form shown in Figs. 6(a) and 6(b) through 8(a) and 8(b). Energy levels convey information better than tables; they can be used to explain the overall features of the observed electron spectra, and, at the same time, provide a guide for more detailed calculations of excited states using any one of the readily available atomic structure computational packages.

From our measured zero-degree energy-gain spectra for Ar^{q+} $(8\leqslant q\leqslant 14)$ on Ar [19], we know that most captures occur with Q values in the 10–50-eV energy range. In this region of Q values, many of the calculated singly, doubly, triply, etc. excited capture states can be quite close in energy, and it may not be possible to identify unambiguously the features in the translational energy gain spectra or Q value distributions with specific single, double, etc. capture states on the basis of energetics alone. (By capture we mean removal of electrons from the target during the collision.)

Figure 6(a) shows a schematic energy-level diagram at infinite separation for the Ar^{8+} + Ar system that goes over to the Ar^{7+} + Ar^{1+} or Ar^{7+} + Ar^{2+} ground state. The measured distribution of Q values for Ar^{8+} on Ar at $79.7q$ eV, is shown in Fig. 9(a) [20]. Single-electron capture occurs for Q values around 12 and 19 eV [21,22]. The lower Q value is associated with capture to $6s$ and $6p$ and the higher value with capture to $5p$, $5d$, and $5f$. These excited states can decay by radiative transitions only. For two electron capture, the possible Q values range from about 25 to 45 eV, Fig. 9(a). This would suggest capture to states bracketed by $(4p)(7s)$ to $(5s)(6p)$ in Table I(a). Given that the $Ar^{7+}+Ar^{2+}$ ground state is about 100 eV below the initial $Ar^{8+}+$ Ar ground state, for the Q in the 25–45-eV energy range, we would expect Auger electrons in the 55–75-eV range. Table I(a) lists nonradiative transition energies for selected $E[8,2,(nl)(n'l')]$ to $E[8,2,(nl)]$ transitions. The energies range from 20 to 80 eV. Although there are only three final states $(3s)$, $(3p)$, and $(3d)$, there is a large number of initial states which leads to a considerable overlap of transition energies to these states. Figure 6(b) shows the highly schematic energy-level diagram for the $Ar^{8+}+$ Ar system that goes to $Ar^{7+}+Ar^{3+}$. In this case we show triple capture to only a few states, $(5s)(5p)^2$, $(5s)^2(5p)$, and $(5p)^3$, that have Q values around 23 eV. These capture states can au-

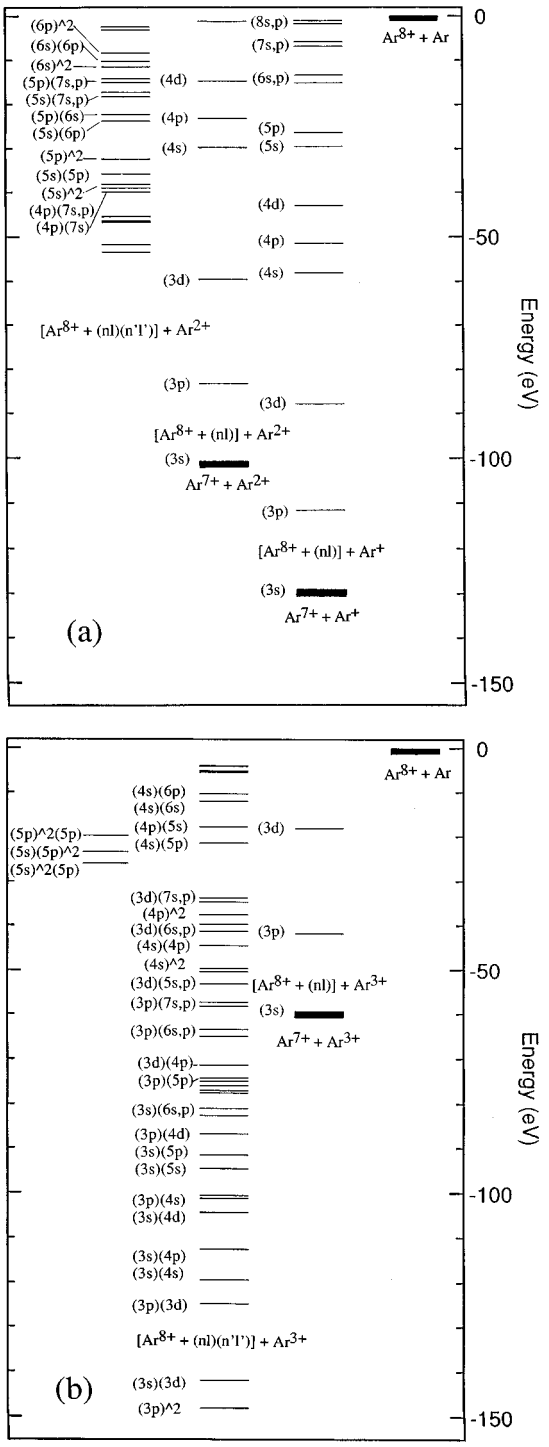

FIG. 6. Total electronic energies of selected states of the $Ar^{8+}+Ar$ collision system at infinite separation after the collision. The energies are plotted with respect to the total electronic energy of the ground state of the $Ar^{8+}+Ar$ system at infinite separation. (a) shows some of the energetically allowed states of $[Ar^{8+}+(nl)]+Ar^{+}$, $[Ar^{8+}+(nl)]+Ar^{2+}$, $[Ar^{8+}+(nl)(n'l')]+Ar^{2+}$. The ground states of the $Ar^{8+}+Ar$, $Ar^{7+}+Ar$, and $Ar^{7+}+Ar^{2+}$ systems are shown with thick lines. (b) shows some of the energetically allowed states of the $[Ar^{8+}+(nl)]+Ar^{3+}$, $[Ar^{8+}+(nl)(n'l)]+Ar^{3+}$, and $[Ar^{8+}+(nl)^2(n'l')]+Ar^{3+}$ systems.

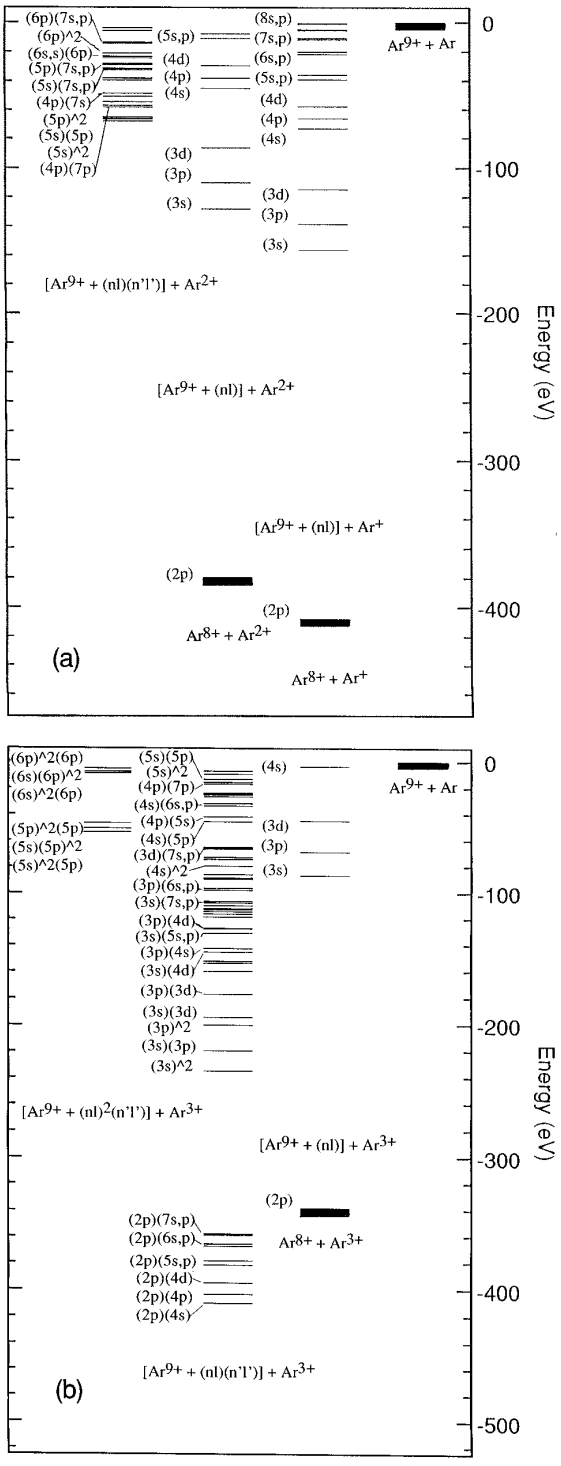

FIG. 7. Total electronic energies of selected final states of the $Ar^{9+}+Ar$ collision system at infinite separation. For more details, see the caption for Fig. 6.

toionize to levels of the doubly excited system just above the energy of the $Ar^{7+}+Ar^{3+}$ ground state. In this case the resulting Auger electrons have energies below 25 eV. If the capture states autoionize to levels below the $Ar^{7+}+Ar^{3+}$ ground state, e.g., to the $(3p)(6s,6p)$ doubly excited states, or to the states below these, Fig. 6(b), then the $E[8,3,(nl)(n'l')]$ states can decay only by a series of radiative

TABLE I. (a) Nonradiative transition energies (in eV) for selected $[Ar^{8+}+(nl)(n'l')]+Ar^{2+}$ to $[Ar^{8+}+(nl)]+Ar^{2+}$ transitions. (b) Nonradiative transition energies (in eV) for selected $[Ar^{8+}+(nl)^2(n'l')]+Ar^{3+}$ to $[Ar^{8+}+(nl)(n'l')]+Ar^{3+}$ transitions.

Q	Initial state	Final state	energy	Final state	energy	Final state	energy
			(a)				
10.2	$(6s)(6p)$	to $(3d)$	49.3	to $(3p)$	73.0	to $(3s)$	90.5
14.1	$(5p)(7p)$		48.1		72.0		89.4
15.0	$(5p)(7s)$		45.4		69.1		86.7
17.2	$(5s)(7p)$		44.5		68.2		85.8
18.2	$(5s)(7s)$		42.4		66.0		83.6
22.2	$(5p)(6s)$		41.3		65.0		82.6
23.7	$(5s)(6p)$		37.4		61.0		78.6
32.3	$(5p)^2$		35.8		59.5		77.1
35.8	$(5s)(5p)$		27.2		50.9		68.5
38.1	$(5s)^2$		23.8		47.5		65.0
39.0	$(4p)(7p)$		21.5		45.1		62.7
40.0	$(4p)(7s)$		20.6		44.3		61.8

Q	Initial State		Final state	energy
	(b)			
19.73	$(5p)^2(5p)$	to	$(3d)(5p)$	30.6
			$(3p)(5p)$	54.5
			$(3s)(5p)$	72.0
23.43	$(5s)(5p)^2$		$(3d)(5p)$	27.0
			$(3p)(5p)$	50.8
			$(3s)(5p)$	68.2
26.04	$(5s)^2(5p)$		$(3d)(5s)$	27.2
			$(3p)(5s)$	50.9
			$(3s)(5s)$	68.6

transitions to the $Ar^{6+}+Ar^{3+}$ ground state ($E[8,3,(3s)^2]$). Since the Q values associated with triple-electron capture are more likely to be around 40 eV or more, the triple-capture states will Auger decay to $[Ar^{8+}+(nl)(n'l')]+Ar^{3+}$ states below the $Ar^{7+}+Ar^{3+}$ state. These states can only decay by radiative transitions to the $Ar^{6+}+Ar^{3}+$ ground state, and we would therefore expect Ar^{6+} scattered projectiles rather than Ar^{7+} projectiles in three-electron capture from the argon target.

The capture of four electrons leading to the $Ar^{7+}+Ar^{4+}$ ground state would be accompanied by even lower-energy Auger electrons. From Fig. 3(a), we see that the maximum observed electron energy is below 90 eV, and there is a pronounced peak around 50 eV. Table I(a) shows that this peak is most likely associated with two-electron capture followed by Auger transitions to the $(3d)$ and $(3p)$ states in $[Ar^{8+}+(nl)]+Ar^{2+}$.

The striking difference between the spectra observed for Ar^{8+} on Ar, Fig. 3(a) and Ar^{9+} on Ar, Fig. 3(b), can be understood from Figs. 7(a) and 7(b) which show the energy-level diagram for the $Ar^{9+}+$ Ar system which eventually goes to the $Ar^{8+}+Ar^{1+}$, $Ar^{8+}+Ar^{2+}$, or $Ar^{8+}+Ar^{3+}$ ground state. The peak in the energy-gain spectrum of Ar^{9+} on Ar [19] corresponds to a Q value around 15 eV. For single-electron capture with this Q value, one would expect capture into $6p$, $6d$, or $6f$ states [21], which in turn can decay only by radiative transitions to the $Ar^{8+}+Ar^{1+}$ ground state. The transfer ionization peak in the energy-gain spectrum [19,21], which corresponds to Q values in the 25–50-eV range, is associated with two-electron capture. From Table II(a), we would expect capture to $(61)(61')$, $(51)(71')$, and $(51)(61')$ states of the projectile. These excited states will in turn decay by nonradiative transitions to the (31) states of the $[Ar^{9+}+(nl)]+Ar^{2+}$ system. The possible electron energies range from 47 to 107 eV, Table II(a). The largest transition energies occur to the $[Ar^{9+}+(3s)]+Ar^{2+}$ state. However, from Fig. 3(a), for the Ar^{8+} on Ar electron spectrum, there is very little intensity above 70 eV, which would rule out transitions to the $[Ar^{8+}+(3s)]+Ar^{2+}$ state, Table I(a). If a similar situation holds for Ar^{9+}, one would not expect electrons with energies greater than 110 eV in the decay of the doubly excited states. This can be readily seen from Fig. 7(a) for $Q=25$ eV. A higher Q value for double capture would result in electrons of even lower energies. This interpretation is consistent with the partial electron energy spectra in coincidence with doubly charged recoil ions measured by Posthumus and Morgenstern [10].

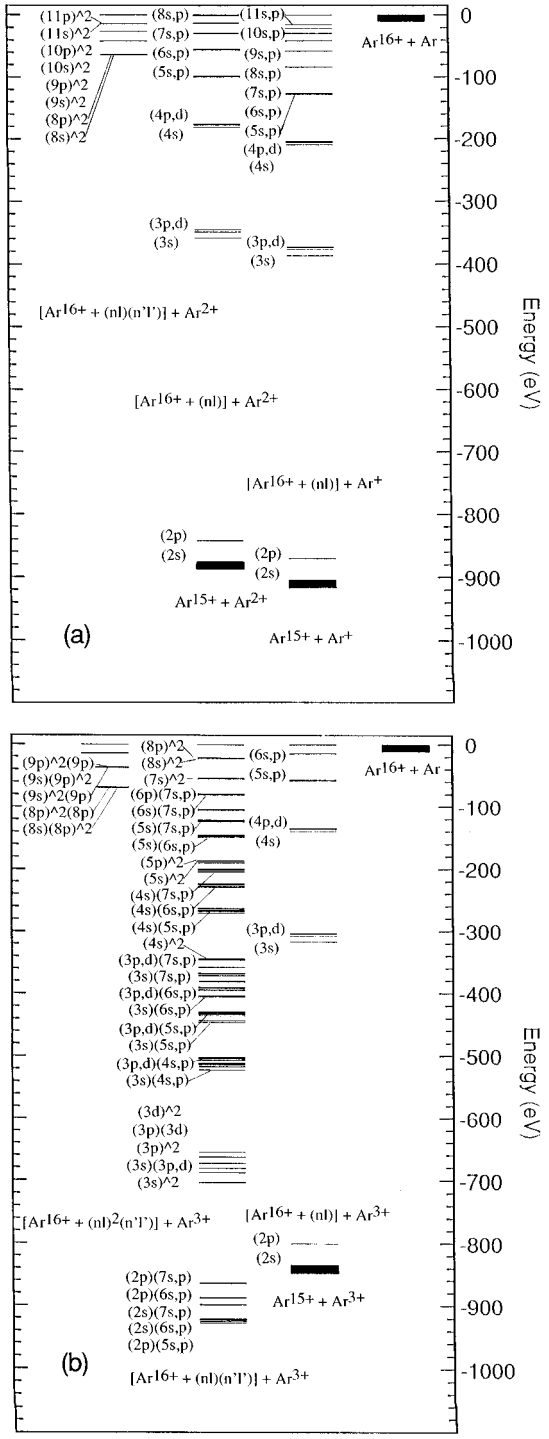

FIG. 8. Total electronic energies of selected final sates of the $Ar^{16+}+Ar$ collision system at infinite separation. For more details, see the caption for Fig. 6.

Figure 7(b) shows energy levels associated with the decay of triply excited states, bracketed by $(5s)^2(5p)$ and $(6p)^3$, formed in three-electron capture. Table II(b) lists nonradiative transition energies for selected $[Ar^{9+}+(nl)^2(n'l')]+Ar^{3+}$ to $[Ar^{9+}+(nl)(n'l')]+Ar^{3+}$ transitions where (nl) is $(5s)$, $(5p)$, $(6s)$, or $(6p)$, since the $(nl)^2(n'l')$ cannot decay to an arbitrary $(n'l')(n''l'')$. One set of quantum numbers in both initial and final states

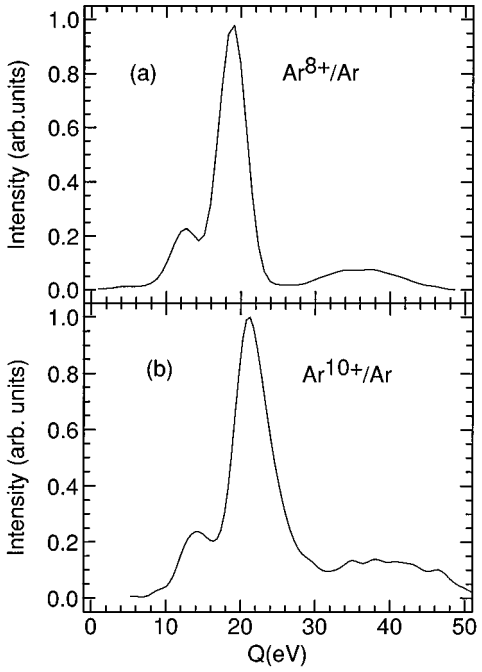

FIG. 9. Distribution of Q values vs Q for (a) Ar^{8+} on Ar, and (b) Ar^{10+} on Ar at $79.7q$ and $92.8q$ eV, respectively. The distribution, taken from Ref. [19], is integrated over all scattering angles.

has to be the same (neglecting higher order Auger processes, which is reasonable). The maximum electron energy in this case is 107 eV, but the bulk of energies is below 90 eV. Table II(c) lists nonradiative transition energies for selected $[Ar^{9+}+(nl)(n'l')]+Ar^{3+}$ to $[Ar^{9+}+(nl)]+Ar^{3+}$ transition energies. If we take the final state (nl) to be $(2p)$, and consider only $(n'l')(n''l'')$ states with $(n'l')$ or $(n''l'')$ the same as in the triply excited capture states, the transition energies range from 186 to 273 eV. Table II(d) lists nonradiative transition energies for selected $[Ar^{9+}+(nl)(n'l')]+Ar^{4+}$ to $[Ar^{9}+(nl)]+Ar^{4+}$ transitions. These 100–200-eV electrons would be observed in the decay of excited states formed in four-electron capture. Figure 3(b) shows that there are fewer electrons in the 80–150-eV range, and that the bulk of electrons falls in the energy ranges discussed above. The partial electron energy spectra in coincidence with the Ar^{3+} recoil show that there are indeed very few electron peaks in the 70–150-eV electron range, and most of the electrons that appear in the spectrum have energies either below 80 eV or between 150 and 260 eV [10].

From Fig. 7(b) we see that it is possible to have transitions from the triply excited capture states $[Ar^{9+}+(nl)^2(n'l')]+Ar^{3+}$ to doubly excited states $[Ar^{9+}+(nl)(n'l')]+Ar^{3+}$ that lie below the $Ar^{8+}+Ar^{3+}$ ground state. These states would then decay by radiative transitions to the $Ar^{7+}+Ar^{3+}$ ground state. However, because of the 300-eV or more transition energy, the Auger rate is small, and it is more likely that the Ar^{7+} (two-electron transfer) projectiles are produced in collisions in which four or more electrons are captured.

The calculated Ar^{10+} on Ar energy-level schemes are very similar to those for Ar^{9+} on Ar, Figs. 7(a) and 7(b).

TABLE II. (a) Nonradiative transition energies (in eV) for selected $[Ar^{9+}+(nl)(n'l')]+Ar^{2+}$ to $[Ar^{9+}+(nl)]+Ar^{2+}$ transitions. (b) Nonradiative transition energies (in eV) for selected $[Ar^{9+}+(nl)^2(n'l')]+Ar^{3+}$ to $[Ar^{9+}+(nl)(n'l')]+Ar^{3+}$ transitions. (c) Nonradiative transition energies (in eV) for selected $[Ar^{9+}+(nl)(n'l')]+Ar^{3+}$ to $[Ar^{9+}+(nl)]+Ar^{3+}$ transitions. (d) Nonradiative transition energies (in eV) for selected $[Ar^{9+}+(nl)(n'l')]+Ar^{4+}$ to $[Ar^{9+}+(nl)]+Ar^{4+}$ transitions.

Q	Initial state	Final state	energy	Final state	energy	Final state	energy
			(a)				
13.5	$(6p)(7s)$	to $(3d)$	72.9	to $(3p)$	96.5	to $(3s)$	114
14.3	$(6s)(7p)$		72.1		95.7		114
21.1	$(6p)^2$		65.4		88.9		107
23.2	$(6s)(6p)$		63.3		86.8		105
24.4	$(6s)^2$		62.0		85.6		104
28.1	$(5p)(7p)$		58.3		81.9		100
29.1	$(5p)(7s)$		57.2		80.9		98.9
31.3	$(5s)(7p)$		55.1		78.7		96.7
32.4	$(5s)(7s)$		54.0		77.6		95.6
37.9	$(5p)(6s)$		48.5		72.0		90.1
39.5	$(5s)(6p)$		46.9		70.5		88.5

Q	Initial state	Final state	energy
	(b)		
8.84	$(6s)^2(6p)$	$(4s)(6s)$	24.6
		$(3d)(6p)$	63.8
		$(3p)(6p)$	87.4
		$(3p)(6s)$	89.1
		$(3s)(6p)$	105
		$(3s)(6s)$	107
50.55	$(5s)(5p)^2$	$(3d)(5p)$	35.4
		$(3d)(5s)$	38.5
		$(3p)(5p)$	59.2
		$(3p)(5s)$	61.5
		$(3s)(5p)$	77.0
		$(3s)(5s)$	80.3

Initial state	Final state	energy
	(c)	
$(4s)(6s)$	$(2p)$	273
$(4p)(5s)$		272
$(4s)(5p)$		272
$(3d)(7p)$		266
$(3d)(7s)$		264
$(3d)(6p)$		259
$(3d)(6s)$		250
$(3d)(5p)$		249
$(3p)(7p)$		242
$(3d)(5s)$		240
$(3p)(7s)$		232
$(3p)(6p)$		231
$(3p)(6s)$		228
$(3s)(7p)$		226
$(3s)(7s)$		226
$(3p)(5p)$		224
$(3p)(5s)$		220
$(3s)(6p)$		211
$(3s)(6s)$		211
$(3d)(4s)$		207
$(3p)(4d)$		196
$(3s)(5p)$		193
$(3s)(5s)$		186

TABLE II. (*Continued*).

Initial state	Final state	energy
	(d)	
$(3p)(4s)$		196
$(3s)(4d)$		193
$(3d)^2$		186
$(3s)(4p)$		184
$(3s)(4s)$		178
$(3p)(3d)$		162
$(3s)(3d)$		144
$(3p)^2$		138
$(3s)(3p)$		119
$(3s)^2$		103

Accordingly, one would expect the spectrum of electrons emitted in Ar^{10+}-on-Ar collisions to be similar to that of Ar^{9+} on Ar, and Fig. 3(c) shows that this is indeed so. The measured distributions of Q values for Ar^{10+} on Ar at $92.8q$ eV is shown in Fig. 9(b) [20]. The distribution is similar to that for Ar^{8+} on Ar. For single-electron capture around $Q=14$ eV, one would expect capture into 71 states, and for $Q\approx 20$ eV into 61 states [21].

For the other Ar^{q+}-on-Ar charge states, one obtains basically the same energy-level structure, and hence the general analysis for Ar^{8+} and Ar^{9+} on Ar should also hold for these charge states. Thus in Fig. 3(f) for Ar^{13+} on Ar, the composite peak between 50 and 80 eV, and the two broad peaks between 150 and 230 eV, can arise from two-electron capture into states with Q values around 30-60 eV, which then autoionize to the $[Ar^{13+}+(41)]+Ar^{2+}$, 50–80 eV, and $[Ar^{13+}+(31)]+Ar^{2+}$ states, 150–240 eV. Triply excited states $[Ar^{13+}+(7s \text{ or } 7p)^2(7s \text{ or } 7p)]+Ar^{3+}$ formed in three-electron capture with Q values around 50 eV can decay by nonradiative transitions to $[Ar^{13+}+(3s \text{ or } 3p)(7s \text{ or } 7p)]+Ar^{3+}$ states, which then decay by nonradiative transitions to $[Ar^{13+}+(2p)]+Ar^{3+}$. The electron energies involved are in the 280–340-eV range. The broad peak extending from 280–330-eV electrons could also be due to nonradiative transitions from $[Ar^{13+}(nl)(n'l')]+Ar^{4+}$ states to the $[Ar^{13+}(31)]+Ar^{4+}$ state. These transitions are at the tail end of the cascade in the decay of quadruply excited states formed in four-electron capture.

Figures 8(a) and 8(b) show the energy levels for the $Ar^{16+}+Ar$ system which goes to $Ar^{16+}+Ar^{1+}$, $Ar^{16+}+Ar^{2+}$, or $Ar^{16+}+Ar^{3+}$. The general considerations applied to the previous collision systems should apply here also, and we would expect more or less the same situation as for the Ar^{13+}-on-Ar system, except for an increase in transition energies. One observes that in Figs. 3(d)–3(i) there is a general trend of the features — they shift to higher energies.

The energy levels shown in Figs. 6(a) and 6(b) through 8(a) and 8(b) are for the collision system at infinite separation. To calculate these energies at different internuclear separations as the colliding partners approach one another, we used the *ab initio* self-consistent field quantum chemistry program GAMESS [23]. Figure 10(a) shows the calculated total electronic energies as a function of internuclear separation for the $Ar^{8+}+Ar$ initial state, and the (arbitrarily chosen) $[Ar^{8+}+(5s)(6s)]+Ar^{2+}$ final state. The calculations were performed using ''standard'' basis sets built into GAMESS, and our own basis set consisting of 11 (s) and eight (p)

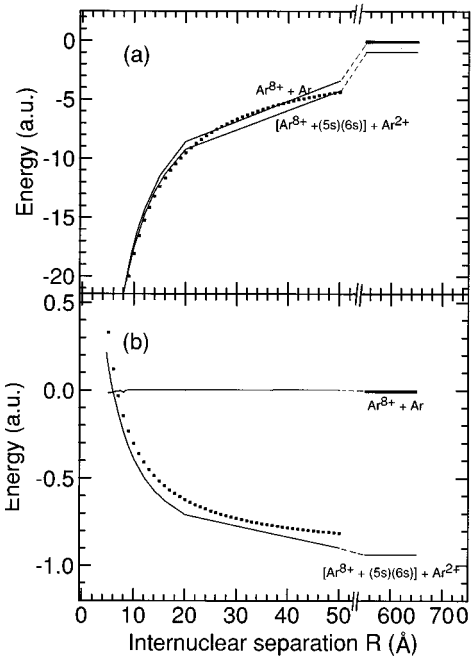

FIG. 10. (a) Plot of the total electronic energy of the initial $Ar^{8+}+Ar$ and final $[Ar^{8+}+(5s)(6s)]+Ar^{2+}$ collision systems as a function of internuclear separation R calculated using GAMESS [23]. The solid squares are the difference between the total electronic energy of the $[Ar^{8+}+(5s)(6s)]+Ar^{2+}$ system at infinite separation and the Coulomb repulsion $18^2/R$ between nuclei. (b) Total energies of the initial $Ar^{8+}+Ar$ and final $[Ar^{8+}+(5s)(6s)]+Ar^{2+}$ collision systems as a function of internuclear separation calculated using GAMESS. The solid dots show the total electronic energy at infinite nuclear separation for the $[Ar^{8+}+(5s)(6s)]+Ar^{2+}$ collision systems plus the ion-ion repulsion $6\times 2/R$. In both (a) and (b), all energies are measured with respect to the initial $Ar^{8+}+Ar$ total electronic ground-state energy.

uncontracted Gaussians fitted to the atomic radial wave functions obtained from Froese-Fischer's code HF86 [18]. We also used uncontracted Gaussians supplemented with a Binning-Curtiss Kr set centered between the Ar nuclei [23]. In all three cases, the results were very similar. The calculations shown in Fig. 10 were done with our basis. In Fig. 10(a) we show the electronic energies, and in Fig. 10(b) the total energies, commonly used to calculate the nuclear motion in the Born-Oppenheimer approximation. The electronic energies are more useful when discussing nonradiative and radiative transitions, as these transitions are easier to visualize in this picture.

If we take the total electronic energy of a particular final state of the collision system at infinite separation, and subtract from it the nuclear repulsion Z^2/R at each internuclear separation R, where Z is the nuclear charge on the centers, we obtain excellent agreement with the energy calculated by GAMESS. For example, using HF86, the calculated total relativistic energies of $[Ar^{8+}+(5s)(6s)]+Ar^{2+}$ and $Ar^{8+}+Ar$ at infinite separation are -1037.19 and -1036.25 a.u., respectively. Subtracting $18^2/R$ a.u. from -0.94 a.u., the energy of the $(5s)(6s)$ state of the collision system with respect to the initial ground-state energy, gives the curve, solid squares, shown in Fig. 10(a). (The agreement is actually better than that shown, since the GAMESS calculations at internuclear separations greater than 20 Å were done at only two points, one of which was at infinity.) Similarly, by adding the repulsive term q_1q_2/R to the final total electronic energy of the collision system at infinite separation also gives a curve that agrees quite well with the GAMESS calculation, Fig. 10(b), solid squares. [q_1 and q_2 are the net charges on the projectile and target in the final state of the collision system. In Fig. 10(b) they are $6+$ and $2+$, respectively.]

Potential curves calculated in this manner are generally referred to as "schematic" in the literature. However, as the above calculation shows, such curves are very good down to the internuclear separations of interest, and, if anything, slightly overestimate crossing radii.

At large internuclear separations, the change in the electronic energy is determined by the Coulomb interaction among the electrons localized on each center, and the ionic charge of the other partner. At smaller internuclear separations, the energies of the single-particle levels are Stark shifted by the electric field produced by the other partner, but this effect is small compared to the above-mentioned Coulomb interaction. As the internuclear separation is reduced further, mixing of the electronic orbitals occurs. When this mixing becomes important, the present calculation breaks down in that the orbitals tend to converge to electronic states other than those of the asymptotic system that one started out with. Interestingly, this occurs at internuclear distances corresponding to those extracted from total charge-transfer cross sections, $\sigma_{\rm tot}$, i.e., distances $\sim\sqrt{\sigma_{\rm tot}/\pi}$.

Finally, since the total electronic energies of the collision system at different internuclear separations R differ from those at infinite separation only by the nuclear repulsion energy Z^2/R, one would expect the energies of Auger electrons emitted in the decay of excited states formed in the collision to be the same as those for an isolated system. At smaller internuclear distances, where the mixing of orbitals is strong, this should no longer be the case.

V. CONCLUSIONS

The spectra of electrons emitted in low energy, Ar^{q+} $(9\leqslant q\leqslant 16)$ on Ar collisions are qualitatively similar. This suggests that they might have a common interpretation. If one assumes that electrons transferred from the target to the projectile during the collision form an excited state that deexcites some time after the collision partners have separated, then the energies of the electrons emitted can be obtained from the total electronic energies of the excited projectile plus recoil ion of charge r referenced with respect to the initial total electronic energy of the projectile-target system. The total electronic energy of the excited projectiles is calculated for configurations that consist of the initial Ar^{q+} core plus one, two, etc. electrons in high-lying unoccupied orbitals. In this work, the total electronic energies of recoil ions of charge r were calculated for the ground state, although excited states of the recoils can easily be obtained. In all cases, the total electronic energies are for the projectile-target system at infinite separation. It should be noted that nonradiative transitions from a given initial to final projectile electron configuration will have different transition energies depending upon the charge state of the recoil ion accompanying the projectile.

With the help of calculated average total electronic energies for different electronic configurations of excited ions plus ground-state recoil ions, the main features observed in Ar^{q+}-on-Ar electron spectra were associated with specific transitions. For Ar^{9+}-on-Ar collisions, an analysis of the electron spectra based on energetics is in qualitative agreement with the electron spectra observed in coincidence with recoil ions of charge $2+$ and $3+$ [10].

The total electronic and total energies of the collision system at different internuclear separations were calculated using the *ab initio* self-consistent field quantum chemistry program GAMESS [23]. It was noted that if one takes the total electronic energy of a particular state of the collision system at infinite separation, and subtracts from it the nuclear repulsion Z^2/R at each internuclear separation R, one obtains excellent agreement with the energy calculated by GAMESS. Similarly, if one adds the repulsive term q_1q_2/R to the total electronic energy of the collision system at infinite separation, the potential-energy curves for different states of the collision system again agree very well with those calculated by GAMESS. The total electronic energies and potential-energy curves so obtained for initial and arbitrary final sates of the collision system agree with the GAMESS calculations down to internuclear separations where appreciable mixing of orbitals takes place.

ACKNOWLEDGMENTS

The help of James Perotti in constructing much of the apparatus used in these experiments is gratefully acknowledged. This work was supported in part by the U.S. Department of Energy, Office of Basic Energy Sciences, Division of Chemical Sciences.

[1] A. Bordenave-Montesquieu, P. Benoit-Cattin, A. Gleizes, A. I. Marrakchi, S. Dusson, and D. Hitz, J. Phys. B **17**, L127 (1984); **17**, L223 (1984).
[2] N. Stolterfoht, C. C. Havener, R. A. Phaneuf, J. K. Swenson, S. M. Shafroth, and F. W. Meyer, Phys. Rev. Lett. **57**, 74 (1986).
[3] M. Mack, J. H. Nijland, P. Van der Stratten, A. Niehaus, and R. Morgenstern, Phys. Rev. A **39**, 3846 (1989).
[4] H. A. Sakaue, Y. Kanai, K. Ohta, M. Kushima, T. Inaba, S. Ohtani, K. Wakiya, H. Suzuki, T. Takayanagi, T. Kambara, A. Danjo, M. Yoshino, and Y. Awaya, J. Phys. B **23**, L401 (1990).
[5] J. Posthumus and R. Morgenstern, J. Phys. B **23**, 2293 (1990).
[6] M. Boudjema, M. Cornille, J. Dubau, P. Moretto-Capelle, A. Bordenave-Montesquieu, P. Benoit-Cattin, and A. Gleizes, J. Phys. B **24**, 1695 (1991); **24**, 1713 (1991), and references therein.
[7] F. Fremont, K. Sommer, D. Leclerc, S. Hicham, P. Boduch, X. Husson, and N. Stolterfoht, Phys. Rev. A **46**, 222 (1992).
[8] J. H. Posthumus, P. Lukey, and R. Morgenstern, J. Phys. B **25**, 987 (1992).
[9] R. Hutton, M. H. Prior, S. Chantrenne, Mau Hsiung Chen, and D. Schneider, Phys. Rev. A **39**, 4902 (1989).
[10] J. H. Posthumus and R. Morgenstern, Phys. Rev. Lett. **68**, 1315 (1992).
[11] J. H. Posthumus and R. Morgenstern, J. Phys. B **25**, 4533 (1992).
[12] J. Vancura and V. O. Kostroun, Phys. Rev. A **49**, 2515 (1994).
[13] J. Vancura, V. Marchetti, and V. O. Kostroun, in *VIth International Conference on the Physics of Highly Charged Ions*, edited by P. Richard, M. Stockli, C. L. Cocke, and C. D. Lin, AIP Conf. Proc. No. 274 (AIP, New York, 1993), p. 113.
[14] V. O. Kostroun, in *International Symposium on Electron Beam Ion Sources and their Applications*, edited by A. Hershcovitch, AIP Conf. Proc. No. 188 (AIP, New York, 1989), pp. 65–81.
[15] J. Vancura, V. J. Marchetti, J. J. Perotti, and V. O. Kostroun, Phys. Rev. A **47**, 3758 (1993).
[16] D. J. Volz and M. E. Rudd, Phys. Rev. A **2**, 1395 (1970).
[17] L. O. Werme, T. Bergmark, and K. Siegbahn, Phys. Scr. **8**, 149 (1973).
[18] C. Froese-Fischer, Comput. Phys. Commun. **43**, 355 (1987).
[19] J. Vancura and V. O. Kostroun (unpublished).
[20] M. Sadilek, J. Vancura, and V. O. Kostroun, J. Phys. Chem. **99**, 15 669 (1995).
[21] E. H. Nielsen, L. H. Andersen, A. Barany, H. Cederquist, J. Heinemeier, P. Hvelplund, H. Knudsen, K. B. MacAdam, and J. Sorensen, J. Phys. B **18**, 1789 (1985).
[22] J. P. Giese, C. L. Cocke, W. Waggoner, L. Tunnell, and S. L. Varghese, Phys. Rev. A **34**, 3770 (1986).
[23] General Atomic and Molecular Electronic Structure System (GAMESS), by M. Dupuis, D. Spangler, and J. J. Wendoloski, National Resource for Computations in Chemistry Software Catalog (University of California, Berkeley, CA, 1980), Program QG01. The version of GAMESS used is described by M. W. Schmidt, K. K. Baldridge, J. A. Boatz, J. H. Jensen, S. Kosski, M. S. Gordon, K. A. Nguyen, T. L. Windus, and S. T. Elbert in Quantum Chem. Program Exchange Bull. **10**, 52 (1990).